

# Idealized large-eddy simulations of nocturnal low-level jets over subtropical desert regions and implications for dust-generating winds

Bernd Heinold,<sup>a,b\*</sup> Peter Knippertz<sup>b,c</sup> and Robert J. Beare<sup>d</sup>

<sup>a</sup>*Leibniz Institute for Tropospheric Research (TROPOS), Leipzig, Germany*

<sup>b</sup>*Formerly at School of Earth and Environment, University of Leeds, UK*

<sup>c</sup>*Institute for Meteorology and Climate Research, Karlsruhe Institute of Technology (KIT), Germany*

<sup>d</sup>*College of Engineering, Mathematics and Physical Sciences, University of Exeter, UK*

\*Correspondence to: B. Heinold, Leibniz Institute for Tropospheric Research, Permoserstraße 15, 04318 Leipzig, Germany. E-mail: heinold@tropos.de

Nocturnal low-level jets (LLJs) are maxima in the wind profile, which often form above the stable nocturnal boundary layer. Over the Sahara, the world's largest source of mineral dust, this phenomenon is of particular importance to the emission and transport of desert aerosol. We present the first ever detailed large-eddy simulations of dust-generating LLJs. Using sensitivity studies with the UK Met Office large-eddy model (LEM), two key controls of the nocturnal LLJ are investigated: surface roughness and the Coriolis force. Functional relationships derived from the LEM results help to identify optimal latitude–roughness configurations for a maximum LLJ enhancement. Ideal conditions are found in regions between 20 and 27°N with roughness lengths  $>0.0001$  m providing long oscillation periods and large jet amplitudes. Typical LLJ enhancements reach up to  $3.5 \text{ m s}^{-1}$  for geostrophic winds of  $10 \text{ m s}^{-1}$ . The findings are largely consistent with results from a theoretical LLJ model applied for comparison. The results demonstrate the importance of latitude and roughness in creating regional patterns of LLJ influence. Combining the functional relationships with high-resolution roughness data over northern Africa gives good agreement with the location of morning dust uplift in satellite observations. It is shown that shear-induced mixing plays an important role for the LLJ evolution and surface gustiness. With decreasing latitude the LLJ oscillation period is longer and, thus, shear-induced mixing is weaker, allowing a more stable nocturnal stratification to develop. This causes a later and more abrupt LLJ breakdown in the morning with stronger gusts, which can compensate for the slower LLJ evolution that leads to a weaker jet maximum. The findings presented here can serve as the first step towards a parametrization to improve the representation of the effects of nocturnal LLJs on dust emission in coarser-resolution models.

**Key Words:** nocturnal low-level jet; boundary-layer transition; large-eddy simulation; dust emission; Sahara; gusts; shear-induced mixing

Received 15 March 2014; Revised 23 September 2014; Accepted 29 September 2014; Published online in Wiley Online Library 27 November 2014

## 1. Introduction

The nocturnal low-level jet (LLJ) is a widespread phenomenon of the night-time boundary layer in many regions. The distinct maximum in the wind speed profile typically forms within the lowest 500 m above ground as the result of an acceleration of horizontal winds to often supergeostrophic velocities. Various possible causes for the nocturnal LLJ formation have been identified. The most common is the mechanism

originally proposed by Blackadar (1957), in which LLJs form in association with the frictional decoupling of air layers above nocturnal inversions. As a response to the perturbed geotriptic balance, the low-level flow accelerates in an inertial oscillation. Subsequent investigations have shown that the nocturnal acceleration and LLJ formation also occur as a consequence of variations in synoptic- or terrain-related baroclinicity (Holton, 1967; Bonner and Paegle, 1970; Shapiro and Fedorovich, 2009).

A number of different approaches have been proposed in the literature for identifying nocturnal LLJs, most of which use criteria for maximum wind speed and height. Others, in addition, require a specific wind speed decrease or vertical wind shear above the nocturnal LLJ (Bonner, 1968; Stensrud, 1996; Fiedler *et al.*, 2013) and/or an increase of the wind speed in the course of the night (May, 1995; Rife *et al.*, 2010). Here, a nocturnal LLJ is defined as a wind speed maximum that forms on top of the nocturnal stable boundary layer and shows appreciable flow acceleration compared to the evening profile. The definition includes but is not limited to supergeostrophic LLJs. A particular wind speed minimum above the jet nose is not required.

The nocturnal LLJ is an important mechanism for atmospheric mixing and transport (Stensrud, 1996) with a large potential to affect aviation (Wittich *et al.*, 1986), air quality (McNider *et al.*, 1988; Mao and Talbot, 2004; Darby *et al.*, 2006), and the wind energy industry (Storm *et al.*, 2009). Observational and modelling studies in recent years have indicated that the nocturnal LLJ also plays an important role in the emission and transport of Saharan mineral dust (Knippertz and Todd, 2012). The nocturnal LLJ momentum gets mixed to the surface during the morning breakdown of the jet and sometimes even through shear-induced nocturnal turbulence (Fiedler *et al.*, 2013). As a result, strong peaks in the near-surface winds and dust raising typically occur from morning to midday. For example, in the Bodélé Depression in Chad, which is the most active single dust source in the world (Koren *et al.*, 2006), dust emission is mainly forced by a topographically enhanced LLJ embedded in the northeasterly harmattan winds (Washington and Todd, 2005). However, nocturnal LLJs have also been shown to be important drivers of dust emission over other parts of the Sahara (e.g. Knippertz, 2008; Schepanski *et al.*, 2009; Fiedler *et al.*, 2013; Heinold *et al.*, 2013; Marsham *et al.*, 2013). According to the model-based climatology by Fiedler *et al.* (2013), 15% of the North African dust emission on annual and spatial average are related to the nocturnal LLJ phenomenon, with a contribution of up to 60% to the total dust uplift over specific areas such as the Bodélé Depression. Once lofted from the surface and mixed across the boundary layer during daytime, dust aerosol remains in the residual layer, where it can be transported within the jet over large distances at night. In summer, the large pressure gradient related to the Saharan heat-low and night-time radiative temperature inversions provide ideal conditions for nocturnal LLJ formation over the Sahara.

For the last 50 years, Blackadar's theory has been extended in various studies and has inspired researches to develop numerous conceptual models and analytical solutions (Thorpe and Guymer, 1977; Beyrich and Klose, 1988; Singh *et al.*, 1993; Shapiro and Fedorovich, 2009; Van de Wiel *et al.*, 2010, VDW10 hereafter). However, despite the clear improvements in the understanding of the nocturnal LLJ phenomenon and its impact on the diurnal cycle of low-level and surface winds, the representation of LLJ characteristics in large-scale atmospheric models is still poor. Fiedler *et al.* (2013), for instance, found a systematic underestimation of the core wind speed and height of nocturnal LLJs in the ERA-Interim reanalysis from the European Centre for Medium-range Weather Forecasts (ECMWF). Studies have suggested that while synoptic-scale dynamics are usually well reproduced, the turbulence parametrization, vertical resolution, and the representation of surface roughness may be insufficient to describe this boundary-layer process (Zhang and Zheng, 2004; Cheinet *et al.*, 2005; Todd *et al.*, 2008; Sandu *et al.*, 2013; Bosveld *et al.*, 2014).

Large-eddy simulations (LESs) can be used to model the nocturnal stable boundary layer (SBL) and LLJ formation provided the grid resolution is high enough to resolve the characteristic flow features. Still, LES modelling of the SBL is challenging (e.g. Beare and MacVean, 2004; Holtslag, 2006; Beare *et al.*, 2006a), and most studies have focused on idealized homogeneous cases with only weakly or moderately stable

conditions because of computational constraints (Zhou and Chow, 2011). One problem is the large domain required to capture the daytime boundary layer, but the small grid length for the night-time SBL. Another problem is non-stationarity during the morning and evening transition, which limits the validity of turbulent flux parametrizations. For this reason, the transitional periods are often omitted in LES studies (Kosović and Curry, 2000; Cuxart and Jiménez, 2007). Bursts of turbulence (intermittent turbulence) during the night, causing sudden vertical mixing, are also difficult to reproduce. Finally, the inertial oscillation itself is a source of shear-generated turbulence and instability in nocturnal boundary layers (Newsom and Banta, 2003; Sun *et al.*, 2004; Mahrt, 2008).

In this study the LES model of the UK Met Office is used for idealized simulations of the nocturnal LLJ phenomenon. To our knowledge, this is the first attempt to conduct LES experiments, covering the entire diurnal cycle of a low-latitude desert boundary layer, which places particular demands on the domain size and grid spacings. The LES results are compared to the theoretical model by VDW10. Sensitivity studies are performed to investigate the two main controls on the LLJ evolution, namely surface friction and the Coriolis force. This provides information on the geographical distribution of the potential strength of nocturnal LLJs. In addition, a major focus of this study is on the link between nocturnal flow enhancement and wind speed variability and gustiness due to the LLJ breakdown during the morning hours. It is also shown how efficient this mechanism potentially is in mobilising dust over different geographical regions. The results are applied to a Saharan context, but without considering the 'disturbing' effects by synoptic forcing or inhomogeneities in surface heating.

## 2. Method

### 2.1. Model description

The nocturnal LLJ simulations were conducted with the UK Met Office large-eddy model (LEM, version 2.4: Gray *et al.*, 2001). The model configuration was largely adapted from Beare *et al.* (2006a) except for the following modifications that account for low-latitude desert boundary-layer conditions. In the Smagorinsky/backscatter subgrid model, the stochastic backscatter was turned off to improve computational efficiency. Following the theoretical analysis of Lilly (1967), a Smagorinsky constant of 0.17 was used, which without backscatter gives a reasonable representation of the SBL. The quadratic conserving centred-difference advection scheme by Piacsek and Williams (1970) was employed for momentum and heat. For simplicity, and in order to reduce the computational expense, the model was configured with zero moisture and the radiation scheme was turned off (Beare *et al.*, 2006a).

The model was forced with a constant geostrophic wind of  $10 \text{ m s}^{-1}$  in the west to east direction. According to the ECMWF ERA-Interim reanalysis for 1989–2008, the westerly component of the 925 hPa geostrophic wind for North Africa is about  $6.7 \pm 10.6 \text{ m s}^{-1}$  on average in June. So, our assumption is in the upper one-third of the climatological range. This was done by design, as only the stronger geostrophic wind speeds are likely to produce winds above typical thresholds for dust emission. Although a value of  $10 \text{ m s}^{-1}$  may occur more often in some regions than in others, no further differentiation is attempted here to allow a straightforward interpretation of the results.

Even though in reality the geostrophic wind veers and decreases with height over North Africa, a height-constant geostrophic wind speed is assumed in the simulations for simplicity. We therefore expect that the model results will not show the typical pronounced maximum of a nocturnal LLJ, while the development in the lowest 100 m, which is the main focus of the article, should not deviate much from reality.

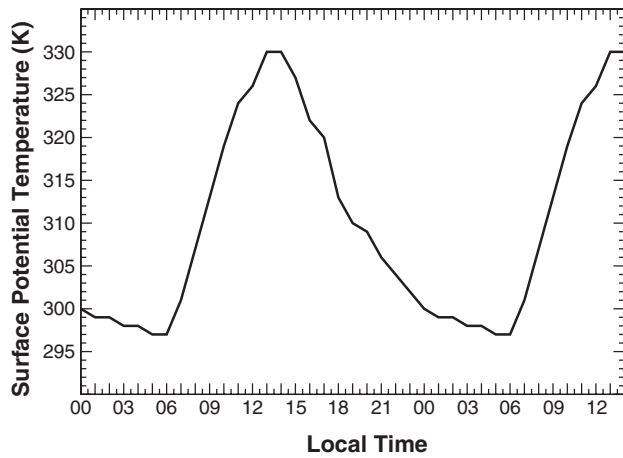


**Figure 1.** Time series of hourly surface potential temperature measured at Ouarzazate/Morocco in June 2006 (Bierwirth *et al.*, 2009), which is used as the lower boundary condition for the LEM runs. Effects of occasional small clouds are excluded by averaging the measurements over the period 1–4 June 2006.

The diurnal cycle of surface temperature from measurements at Ouarzazate/Morocco ( $30.93^{\circ}\text{N}$ ,  $6.90^{\circ}\text{W}$ ) in June 2006 (Bierwirth *et al.*, 2009) was used as lower boundary condition (Figure 1) following Basu *et al.* (2008). Here, temperature observations for the period 1–4 June 2006 were combined so that the effects of occasional small clouds average out. The diurnal cycle shows a minimum of 297 K during the 2 h before sunrise, which is around 0600 local time (LT). The maximum daytime temperature of 330 K is reached in the early afternoon between 1300 and 1400 LT. Note the abrupt and steep increase in surface temperature during the morning hours in contrast to the more gradual cooling in the evening. This very sharp increase in surface heating, which is typical for dry, sparsely or non-vegetated soils, causes the daytime convective boundary layer (CBL) to grow fast and favours an abrupt and intense morning breakdown of the LLJ.

The prescribed diurnal variations of surface temperature correspond well to satellite and ground observations elsewhere in the Sahara and Sahel (e.g. Pinker *et al.*, 2007; Jin and Dickinson, 2010). The satellite-based climatology from Jin and Dickinson (2010) shows daytime surface temperatures up to 310–320 K and night-time values up to 290–300 K with a diurnal range of 20–25 K (larger in mountain areas) over the Sahara and other subtropical desert regions. In reality, the surface temperature depends on the evolution of the boundary layer, and vice versa. Prescribing surface temperatures, therefore, might lead to an incorrect representation of the surface decoupling and the resulting fast radiative cooling of the surface for some low roughness lengths.

The initial wind profile used was set to the geostrophic value above the surface. The potential temperature was initialised with an idealized profile for stable conditions with a vertical gradient of potential temperature of  $0.003 \text{ K m}^{-1}$  (starting from 302 K at the first vertical level). In order to allow the development of turbulence, a random perturbation of  $\pm 0.1 \text{ K}$  was imposed on the potential temperature in the lowest 50 m. A layer damping was applied to the horizontal means of prognostic variables above 6000 m to reduce the reflection of gravity waves at the domain top.

The model runs were performed for 36 h from 0000 LT. The horizontal domain size was  $\Delta x = \Delta y = 4800 \text{ m}$  with  $12.5 \text{ m}$  grid spacing ( $384 \times 384$  grid cells), giving a big enough domain for the CBL and a sufficiently high resolution for the SBL (Beare *et al.*, 2006b). The domain had a vertical extent of 6500 m with 180 irregularly spaced grid levels. The level depth was about 5 m in the lowest 100, 10 m in the next 300, 25 m up to 2000 m height, and then increased to 100 m at the domain top. For the sensitivity tests, the LEM was run (i) at fixed latitudes of  $10^{\circ}\text{N}$  (Coriolis parameter  $f = 0.25 \times 10^{-4} \text{ s}^{-1}$ ),

$20^{\circ}\text{N}$  ( $f = 0.50 \times 10^{-4} \text{ s}^{-1}$ ) and  $30^{\circ}\text{N}$  ( $f = 0.73 \times 10^{-4} \text{ s}^{-1}$ ) for a set of six surface roughness lengths for momentum and heat, respectively, ranging from  $1.0 \times 10^{-5}$  to  $1.0 \text{ m}$ ; (ii) for a fixed roughness length of  $z_0 = 0.1 \text{ m}$ , for eight runs performed at latitudes between  $5$  and  $35^{\circ}\text{N}$  ( $f = 0.13\text{--}0.83 \times 10^{-4} \text{ s}^{-1}$ ). The surface roughness is very low over wide areas in the Saharan desert (Prigent *et al.*, 2012), and some values of  $z_0$  considered here are larger than what is typically observed. Still, roughness lengths on the order of  $1.0 \text{ m}$  can be found in desert mountain regions.

## 2.2. Theoretical model

In addition to the LEM, we use the theoretical model by VDW10, which describes the development of an LLJ resulting from the nocturnal inertial oscillation. The model is an extension of the original theory from Blackadar (1957), which additionally accounts for turbulent friction within the nocturnal boundary layer parametrized by using a constant friction term. As a consequence, the nocturnal wind profile oscillates around a nocturnal equilibrium wind vector instead of the geostrophic wind vector as in Blackadar's model. Compared to existing exact analytical solutions (Shapiro and Fedorovich, 2010, and references therein), the model by VDW10 is easy to use, in particular as no turbulence closure is required. The model provides vertically continuous, time-dependent wind profiles on the basis of observed or modelled data as initial conditions. The nocturnal evolution of the zonal ( $U$ ) and meridional ( $V$ ) wind speed components in time is given by:

$$U - U_{\text{eq}} = (V_0 - V_{\text{eq}}) \sin(ft) + (U_0 - U_{\text{eq}}) \cos(ft), \quad (1)$$

and

$$V - V_{\text{eq}} = (V_0 - V_{\text{eq}}) \cos(ft) - (U_0 - U_{\text{eq}}) \sin(ft), \quad (2)$$

where  $U_0$  ( $V_0$ ) and  $U_{\text{eq}}$  ( $V_{\text{eq}}$ ) represent the initial and equilibrium zonal (meridional) velocity profiles (see VDW10 for a detailed derivation), and  $t$  is the time of oscillation after frictional decoupling. Here, the 1900 LT wind profiles as computed by the LEM are used for initialisation. The equilibrium wind vector is approximated by a simple Ekman-balanced model as proposed by VDW10:

$$U = U_g - U_g e^{-\gamma z} \cos(\gamma z) - V_g e^{-\gamma z} \sin(\gamma z), \quad (3)$$

and

$$V = V_g - V_g e^{-\gamma z} \cos(\gamma z) + U_g e^{-\gamma z} \sin(\gamma z), \quad (4)$$

where  $\gamma = \sqrt{f/2K}$  ( $\text{m}^{-1}$ ),  $K$  is the eddy diffusivity ( $\text{m}^2 \text{ s}^{-1}$ ), and  $f$  the Coriolis parameter ( $\text{s}^{-1}$ ). Here, the eddy diffusivity in the surface layer at 2400 LT is also taken from the LEM runs, respectively. The calculations with the theoretical model are performed for different latitude–roughness configurations analogously to the large-eddy simulations (see section 2.1).

## 3. Example of an idealized nocturnal LLJ case

The evolution of a nocturnal LLJ in the idealized large-eddy simulations is presented for the run with  $z_0 = 0.01 \text{ m}$  and  $20^{\circ}\text{N}$  latitude as an example. The CBL freely develops during the first simulation day and reaches a top height of 5000 m, a typical value for the Sahara (Gamo, 1996; Cuesta *et al.*, 2009).

For the period from 1700 to 0900 LT, mean profiles of potential temperature, wind speed, as well as heat and momentum fluxes in Figure 2(a–f), respectively, show the transition from convective to SBL conditions and vice versa. At 1700 LT, about 1 h before sunset, the potential temperature profile still exhibits a superadiabatic lapse rate within the surface layer due to the strongly heated surface (Figure 2(a)). Strong turbulent

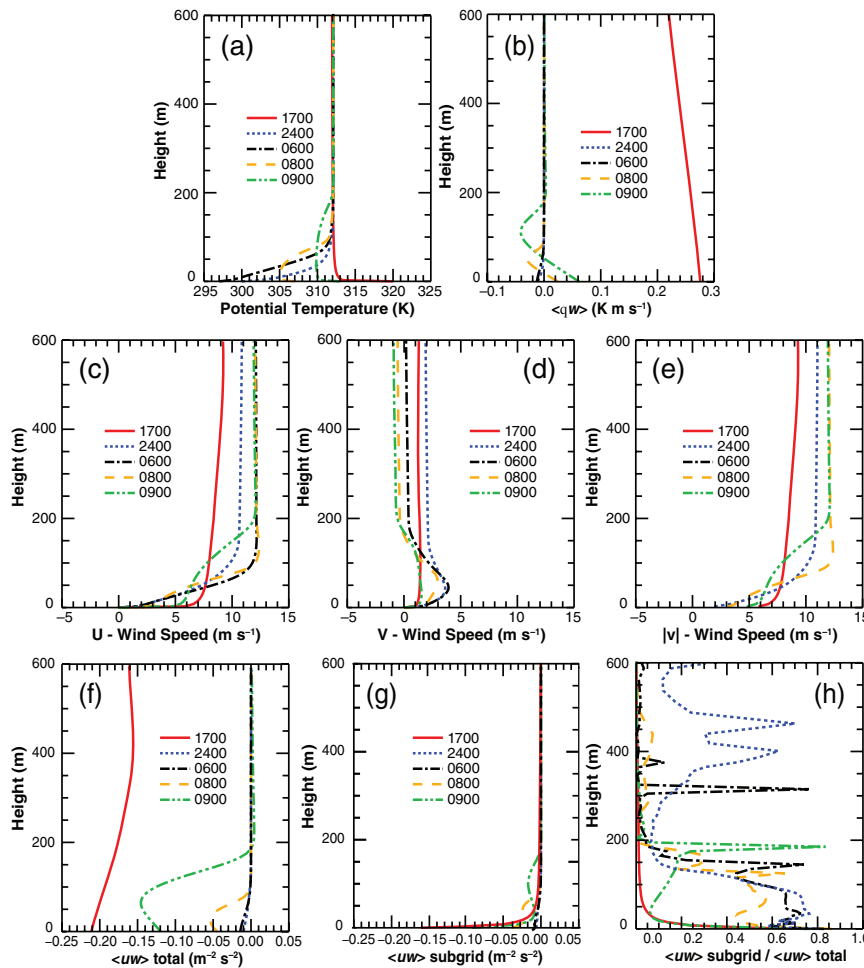


**Figure 2.** Vertical profiles of domain-averaged (a) potential temperature, (b) total heat flux, (c–e) wind speed ( $U$ - $V$ -components and magnitude), (f,g) total and subgrid-scale zonal momentum flux, respectively, and (h) ratio of subgrid to total (subgrid and grid scale) zonal momentum flux for the run with  $z_0 = 0.01$  m at latitude  $20^\circ\text{N}$  from  $t = 17$  h (1700 LT) to 33 h (0900 LT).

mixing occurs as indicated by the momentum fluxes shown in Figure 2(f). The profiles of potential temperature and velocity show constant values with height in the deep convective mixed layer (Figure 2(a,d)). During the evening transition, radiative cooling begins to stabilise the lowest atmospheric layers and the SBL forms. At midnight, very stable conditions prevail with a vertical gradient of potential temperature of  $0.2 \text{ K m}^{-1}$  within the lowest 50 m (Figure 2(a)). With increasingly stable conditions, the residual layer becomes decoupled from surface friction in the course of the night as evident from the momentum fluxes, which are strongly reduced near the surface and drop to zero above the SBL top at 100 m height (Figure 2(f)). As a result of the interrupted geostrophic–antitriptic equilibrium, an inertial oscillation develops, in which the flow is accelerated to a supergeostrophic jet above the SBL (Figure 2(b–d)). Note that, in contrast to many observations, a distinct jet maximum is missing in the magnitude of wind speed, as the acceleration extends over the entire residual layer. This is largely due to the prescription of constant geostrophic wind with height, i.e. barotropicity. The nose of the meridional wind profile within the SBL should not be mixed up with the LLJ as it results from the Ekman spiral (Figure 2(c)). The jet further intensifies during the night from about  $11.0 \text{ m s}^{-1}$  at 2400 LT to  $12.0 \text{ m s}^{-1}$  at 0600 LT.

A corresponding wind hodograph at jet level (see red line in Figure 4(a), further discussed below) shows that the changes in the wind components in Figure 2(b,c) are consistent with a clockwise rotation of the wind profile. The hodograph has the shape of the segment of a circle, suggesting that the flow is effectively decoupled. According to theory, the maximum enhancement of wind speed occurs at a little less than half the oscillation period ( $\tau_{1/2} = \pi/f$ ), which is 17.5 h for this run ( $20^\circ\text{N}$ ;  $f = 0.50 \times 10^{-4} \text{ s}^{-1}$ ). As the period between sunset and sunrise

is about 12 h by prescription in this run, the decoupled period is shorter, and the nocturnal LLJ reaches its peak strength at 0800 LT with a wind speed of  $12.5 \text{ m s}^{-1}$  and a slightly pronounced nose at 125 m agl (Figure 2(d)). At this time, the profile of momentum flux (Figure 2(f)) already shows the intensification of turbulent mixing induced by the morning surface heating (Figure 2(a)). The mixing, however, remains limited to less than the height of the former SBL. One hour later, the negative peak of the momentum flux profile is about three times larger and reaches up to 200 m above ground level (agl), which means that turbulence has eroded the nocturnal inversion. As a result, LLJ momentum is mixed to the surface, leading to the breakdown of the jet (Figure 2(d,f)). The rapid development during the morning transition of the boundary layer is also illustrated in Figure 3, showing cross-sections of vertical velocity through the model domain between 0600 and 0900 LT. The rapidly growing extent of up- and downdraughts indicates the change from the small-scale turbulent structures in the SBL to the large plumes that dominate the CBL flow.

Due to the highly idealized model set-up, a comparison to LLJ observations here is not meaningful. Instead we provide some level of model evaluation by including a comparison to the dust emission climatology from Schepanski *et al.* (2007, 2012) in section 5.2. Overall, the results suggest that frictional decoupling during the evening transition of the boundary layer and the onset of turbulent mixing after sunrise are well described. With grid spacings of 12.5 m, the turbulent structures in the evening and morning hours are explicitly modelled, except in the lowest layer. This can be seen in Figure 2(g), showing subgrid momentum fluxes, which, near the surface, are on the same order of magnitude as the grid-scale fluxes at higher levels. The subgrid-scale fraction of turbulent fluxes increases to 75% within

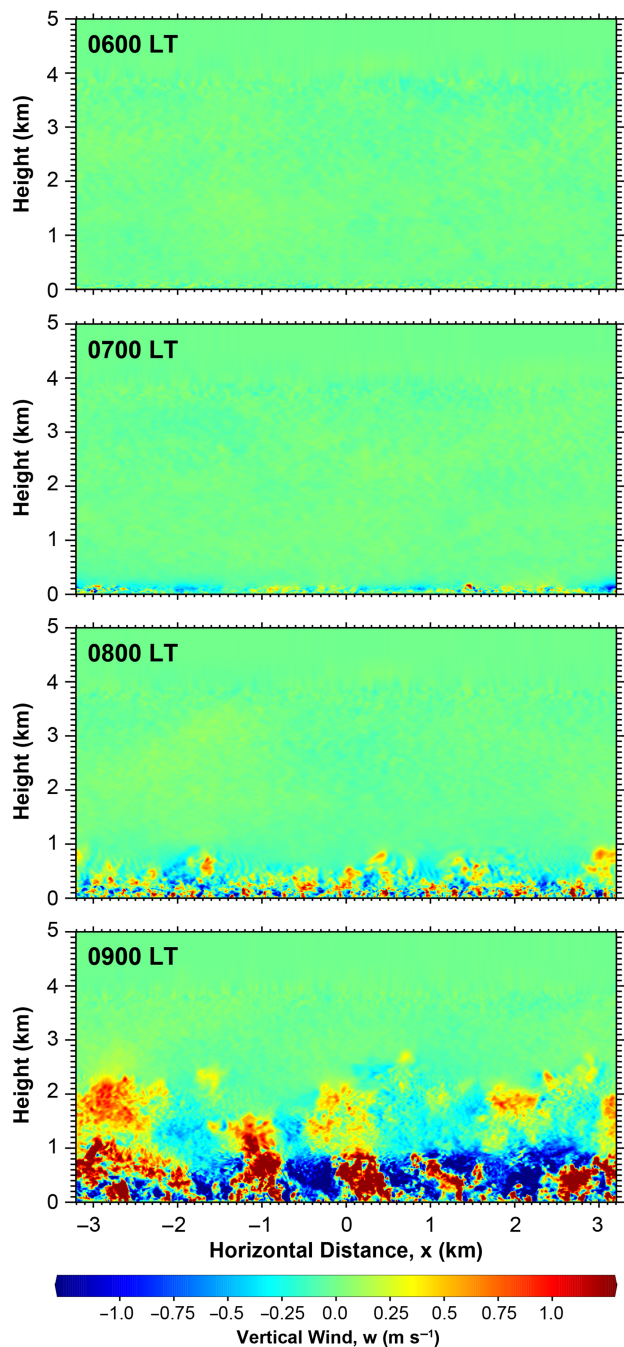


**Figure 3.** Vertical cross-sections of the instantaneous vertical velocity through the domain centre along the geostrophic wind vector blowing from left to right. The results are shown for the run with  $z_0 = 0.01 \text{ m}$  at latitude  $20^\circ\text{N}$  from  $t = (a)$  30 h (0600 LT) to (d) 33 h (0900 LT) showing the morning transition of the boundary layer.

the nocturnal SBL (Figure 2(h)). However, note that most of the peaks in Figure 2(h) result from dividing small numbers by small numbers (cf. Figure 2(f,g)). Still the LEM is able to sustain resolved turbulent motion, but the mixing by the subgrid scheme is not too high to prevent the decoupling of atmospheric layers and allows modelling a well-defined nocturnal SBL. The grid spacing here is still quite large for an SBL owing to the large domain required for the CBL. If accessible, higher resolutions would probably give a shallower boundary layer ((Beare and MacVean, 2004; Beare *et al.*, 2006a), and so the jet might be decoupled even more.

#### 4. Dependence on surface roughness and Coriolis parameter

##### 4.1. LLJ enhancement and supergeostrophic factor

In the following, the main controls on the nocturnal LLJ evolution, more precisely the inertial oscillation, are investigated. The

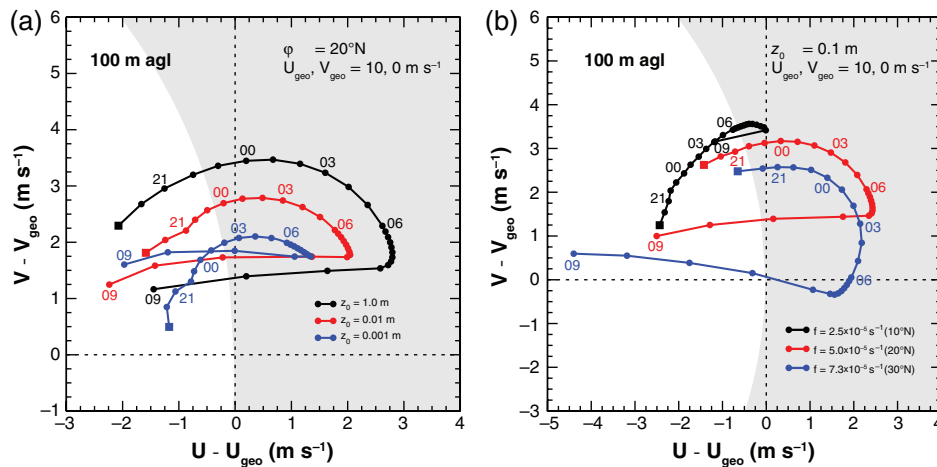
amplitude of the oscillation is a function of the ageostrophic wind component before the start of decoupling, which depends on the background pressure gradient, the latitudinal location (Coriolis parameter) and surface friction. In this study, a uniform geostrophic wind is assumed for all runs, reducing the set of controlling parameters to the roughness length and the Coriolis parameter. Their effects are analysed in hodographs of the ageostrophic wind components at LLJ level in Figure 4.

Figure 4(a) shows the results of the model runs for  $20^\circ\text{N}$  with surface roughness lengths of 1.0, 0.01 and 0.001 m, respectively. In each case, the ageostrophic wind vector describes a segment of a circle in the course of the night, indicating an almost undisturbed oscillation with highly supergeostrophic winds during the early morning hours (grey shading in Figure 4(a)). The abrupt turn in the curve around 0800 LT nicely shows the breakdown of the nocturnal LLJ and the rapid transition back to a subgeostrophic flow. With increasing surface roughness, there is an increase in the ageostrophic wind speed, i.e. the oscillation amplitude, and the angle between the absolute and geostrophic wind vector, while the absolute wind speed decreases. For the 1900 LT values in Figure 4(a), the ageostrophic wind increases from about  $1.3 \text{ m s}^{-1}$  for  $z_0 = 0.001$  to  $3.1 \text{ m s}^{-1}$  for  $z_0 = 1.0 \text{ m}$ . The absolute wind speed decreases from  $8.8$  to  $8.3 \text{ m s}^{-1}$ . Rougher surfaces exert a stronger frictional force, leading to a larger departure from geostrophy, and thus cause an inertial oscillation with higher amplitude than smoother surfaces.

The surface roughness also influences the pace of the LLJ evolution. Given the larger LLJ amplitude, supergeostrophic conditions occur about 3 h earlier in the model run for  $z_0 = 1.0 \text{ m}$  (2230 LT) than in the one for  $z_0 = 0.001 \text{ m}$  (0200 LT). In addition, the breakdown of the LLJ takes place slightly later, the larger the roughness length is in the model. It occurs around 0745 LT for  $z_0 = 0.001 \text{ m}$  and around 0815 LT for  $z_0 = 1.0 \text{ m}$ . This is likely caused by the higher near-surface wind speeds over smooth terrain and the associated stronger shear-induced mixing lowering the atmospheric stability (see section 5 for a more detailed discussion). The results for the smaller two roughness lengths show slight deviations from an idealized oscillation during the evening and early night. This is most likely an artefact of the model, and is related to a change from an early oscillation, developing during the evening transition, to a later one, which newly starts from a later wind profile when the resolved regime changes towards a mainly subgrid-scale driven flux representation. The break occurs earlier the larger the roughness length is in the model. This deviation, however, remains small and does not affect the overall conclusions.

Hodographs from the model runs at  $10^\circ\text{N}$  ( $f = 0.25 \times 10^{-4} \text{ s}^{-1}$ ),  $20^\circ\text{N}$  ( $f = 0.50 \times 10^{-4} \text{ s}^{-1}$ ), and  $30^\circ\text{N}$  ( $f = 0.73 \times 10^{-4} \text{ s}^{-1}$ ) latitude with  $z_0 = 0.1 \text{ m}$  show the dependency on the Coriolis parameter (Figure 4(b)). As mentioned above, the Coriolis force controls the starting point, i.e. the magnitude of ageostrophic wind components at the time of decoupling, and the period of the inertial oscillation. According to Ekman theory, the absolute wind increases and the ageostrophic wind decreases with increasing latitude. The evening jet-level winds at 1900 LT in fact show an increase in the absolute wind speed from about  $7.7 \text{ m s}^{-1}$  at  $10^\circ\text{N}$  to  $9.7 \text{ m s}^{-1}$  at  $30^\circ\text{N}$ . However, the behaviour of the ageostrophic wind speed is less clear throughout the set of runs with values of  $2.7 \text{ m s}^{-1}$  ( $10^\circ\text{N}$ ),  $3.0 \text{ m s}^{-1}$  ( $20^\circ\text{N}$ ) and  $2.6 \text{ m s}^{-1}$  ( $30^\circ\text{N}$ ). The hodograph that stands out is the one for  $10^\circ\text{N}$ , indicating that the Coriolis force is already too weak for the geotriptic balance to establish during daytime. At those low latitudes, the pressure gradient force is almost solely balanced by the boundary-layer drag, and turbulent mixing tends to bring the absolute wind back close to the geostrophic value. In order to rule out that this is due to setting the initial wind profile to the geostrophic wind, the model run for  $10^\circ\text{N}$  was repeated using an Ekman profile instead, however, with an almost identical result.

For an ideal oscillation, periods of 69.8, 34.9 and 23.9 h are calculated for 10, 20 and  $30^\circ\text{N}$ , respectively. This means that in the



**Figure 4.** Hodographs of ageostrophic velocity components at LLJ level (ca. 100 m agl) for runs with different (a) roughness lengths and (b) Coriolis parameters (i.e. different latitudinal locations). A geostrophic wind speed of  $[U_{\text{geo}}, V_{\text{geo}}] = [10, 0]\text{ m s}^{-1}$  is prescribed in the simulations. Each symbol represents an hourly (1900 to 0600 LT) and quarter-hourly (0600–0900 LT) value, respectively. Squares indicate the evening profile at 1900 LT. Grey shaded areas mark the range of supergeostrophic wind speeds.

decoupled period, only one quarter of the oscillation is completed at  $10^\circ\text{N}$  latitude, while it is about half at  $30^\circ\text{N}$ . The hodographs in Figure 4(b) confirm the differences in the pace of LLJ evolution. Supergeostrophic wind speeds are reached at about 1930 LT at  $30^\circ\text{N}$  latitude and only at 0630 LT at  $10^\circ\text{N}$ . Flow acceleration reaches a maximum when the ageostrophic vector points in the direction of the equilibrium (geostrophic) wind vector, which is the case after just under half the oscillation period.

The highest amount of momentum for downward mixing is available, and therefore peak near-surface winds occur, when the jet maximum coincides with the nocturnal LLJ breakdown. This is about the case for  $20^\circ\text{N}$ , where the jet breaks down at about 0800 LT. The breakdown of the nocturnal LLJ at  $10^\circ\text{N}$  occurs at about 0845 LT and 0730 LT at  $30^\circ\text{N}$ , even though all runs are forced with the same surface temperature evolution (Figure 4(b)). The difference in the time of the LLJ breakdown results from wind shear, which is stronger with a faster jet development, such as at  $30^\circ\text{N}$  latitude. Shear-driven turbulence reduces the static stability in addition to the surface heating after sunrise, and can cause an early termination of the nocturnal decoupling (see details in section 5).

#### 4.2. Functional relationship

To further quantify the strength of a nocturnal LLJ mainly formed due to an inertial oscillation, the quantity ‘potential LLJ enhancement’ ( $JE$ ) is introduced. It is defined as the difference of wind speed at jet level between 1900 and 0600 LT on the following day.  $JE$  describes the acceleration of the low-level flow due to the nocturnal inertial oscillation. In general, as shown in Figure 4, large values of  $JE$  are associated with high LLJ momentum, which can be mixed towards the surface in the morning, depending on roughness length. Since the actual LLJ breakdown occurs 1.5–3 h after sunrise, the LLJ evolution can continue. Therefore, we expect a slight under- or overestimation of the LLJ enhancement depending on whether the jet further strengthens ( $10^\circ\text{N}$ ) or already weakens ( $30^\circ\text{N}$ ), respectively (Figure 4(b)). In addition, the LLJ strength in the morning is estimated relative to the geostrophic wind using the ‘supergeostrophic factor’ (SGF), which is the difference between the jet wind speed at 0600 LT and the geostrophic wind.

Figure 5(a,b) show  $JE$  for the simulations with different roughness lengths at latitude  $20^\circ\text{N}$  and with a roughness length of  $0.1\text{ m}$  for different latitudinal locations (Coriolis parameters).  $JE$  increases approximately logarithmically with the roughness length from  $1.44\text{ m s}^{-1}$  at  $z_0 = 1.0 \times 10^{-5}\text{ m}$  to  $4.46\text{ m s}^{-1}$  at  $z_0 = 1.0\text{ m}$  (Figure 5(a)). From a latitude of  $5^\circ\text{N}$ ,  $JE$  gradually increases from  $0.84\text{ m s}^{-1}$  to a maximum of  $3.71\text{ m s}^{-1}$  at  $25^\circ\text{N}$ ,

respectively, and then decreases again to a value of  $1.58\text{ m s}^{-1}$  at  $35^\circ\text{N}$  latitude (Figure 5(b)). This peak in LLJ enhancement with latitude is the result of an optimal balance between inertial and diurnal time-scales.

Through fitting we obtain functional relationships of  $JE$  for surface roughness ( $z_0$ ) and latitude ( $\varphi$ ):

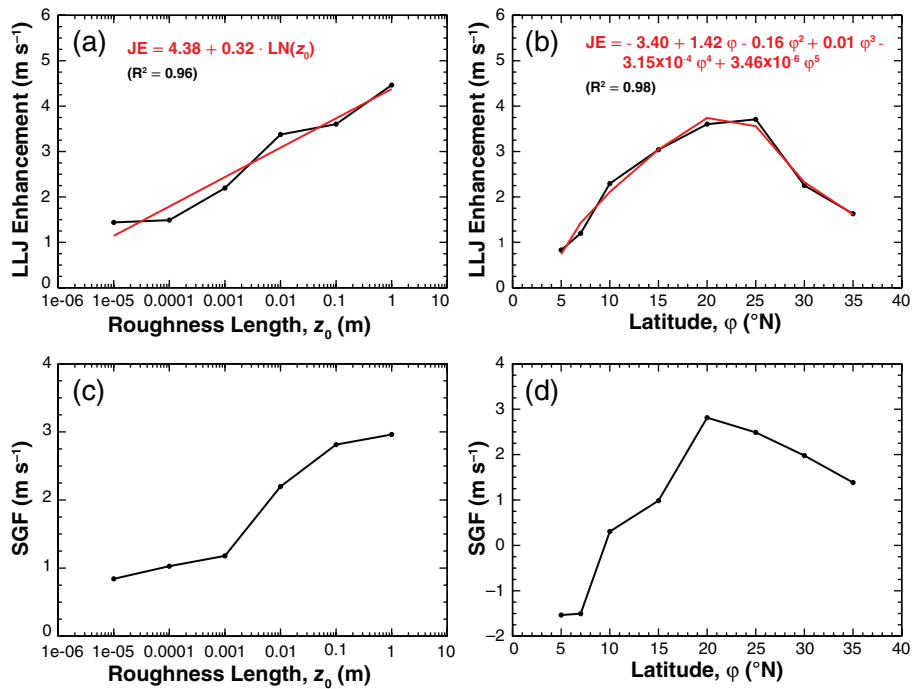
$$JE_{z_0} = 4.38 + 0.32 \cdot \ln(z_0), \quad (5)$$

$$\begin{aligned} JE_\varphi = & -3.40 + 1.42\varphi - 0.16\varphi^2 + 0.01\varphi^3 \\ & - 3.15 \times 10^{-4}\varphi^4 + 3.46 \times 10^{-6}\varphi^5. \end{aligned} \quad (6)$$

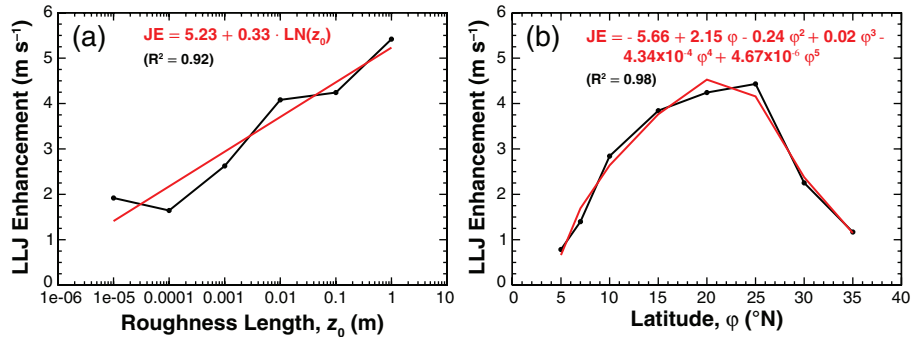
Considering the findings above, it is not surprising that Eq. (5) has a logarithmic dependency on  $z_0$  as the boundary-layer wind does in general. A more complex relation between  $JE$  and latitude is given by the fifth-order polynomial in Eq. (6). The shape of the curve, however, is consistent with a combination of triangular functions like the latitudinal dependence of the Coriolis parameter.

A similar dependency on surface roughness and latitude is found for the supergeostrophic factor with values ranging between  $-1.5$  and  $3.0\text{ m s}^{-1}$  (Figure 5(c,d)). The SGF is a more direct measure of the absolute jet maximum at 0600 LT relative to the geostrophic wind. It is based on the idea that the nocturnal equilibrium wind vector, around which the nocturnal wind profile oscillates, can be approximated by the geostrophic wind profile. The analysis reveals that the inertial oscillation generally leads to a flow acceleration compared to the evening profile, while a supergeostrophic jet does not form in every case, as indicated by negative values of SGF for LEM runs at latitudes south of  $7^\circ\text{N}$ . There is a large agreement between Figure 5(b and d) for latitudes higher than  $20^\circ\text{N}$ . However, a stronger decrease to lower latitudes is found for the SGF. This is because, for the given initial wind profile, the pressure gradient force at higher latitudes is larger and, therefore, the evening wind is closer to the geostrophic value compared to latitudes less than  $20^\circ\text{N}$ .

In addition to the large-eddy simulations, the theoretical model by VDW10 is used to describe the evolution of the nocturnal LLJ. The 1900 LT wind profile and eddy diffusivity in the surface layer at 2400 LT from the respective LEM run serve as input parameters (for more details see section 2.2). The prescribed eddy diffusivity has to be small with values in the order of  $0.025\text{ m}^2\text{s}^{-1}$ . Generally, the nocturnal LLJ evolution in the wind profiles agrees well with the LES results, indicating that flow acceleration in the upper layers almost ideally follows the inertial oscillation in the LES runs. On the other hand, this confirms that an Ekman profile is a good representation for the nocturnal equilibrium wind (VDW10).



**Figure 5.** Modelled LLJ enhancement and supergeostrophic factor (SGF) shown as function of (a,c) surface roughness at latitude  $20^{\circ}\text{N}$  and (b,d) latitude (Coriolis parameter) for  $z_0 = 0.1\text{ m}$  (black line). The LLJ enhancement is defined as the difference of wind speed at LLJ level between  $t = 30\text{ h}$  (0600 LT) and  $19\text{ h}$  (1900 LT). SGF is the difference between the jet-level wind speed at  $t = 30\text{ h}$  (0600 LT) and the geostrophic wind. Red lines show the regression lines given by the inset equations, with the coefficient of determination ( $R^2$ ).



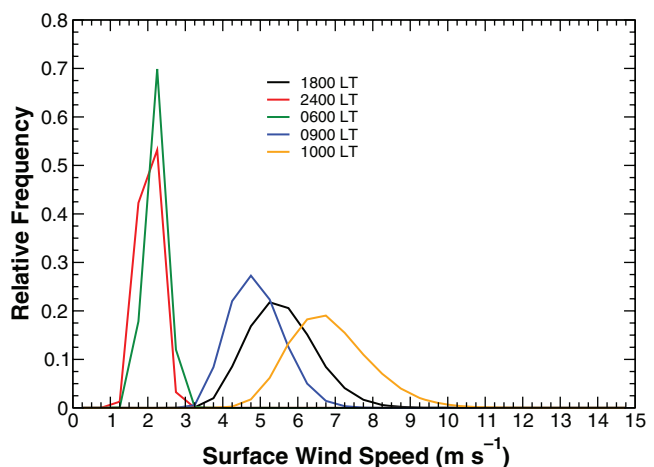
**Figure 6.** LLJ enhancement as function of (a) surface roughness at latitude  $20^{\circ}\text{N}$  and (b) latitude (Coriolis parameter) for  $z_0 = 0.1\text{ m}$  (black line) calculated from the theoretical model by VDW10 (see details in section 2.2). Red lines show the regression lines given by the inset equations, with the coefficient of determination ( $R^2$ ).

Figure 6(a,b) shows the nocturnal LLJ enhancement as functions of surface roughness and latitude, respectively, as calculated using the VDW10 model. The results from the theoretical model are very similar to those from the LEM runs shown in Figure 5, including similar regression equations (red lines in Figure 6). The values of JE, however, are slightly higher than in the LES results, particular for strong enhancements. In Figure 6(b), for example, the maximum at  $25^{\circ}\text{N}$  is about  $4.50\text{ m s}^{-1}$  instead of  $3.71\text{ m s}^{-1}$  (cf. Figure 5(b)). A reason for this could be that, for high enhancement values, shear-induced mixing already dissipates LLJ momentum in the second half of the night. This change in eddy diffusivity, of course, is not considered in the theoretical model, leading to an overestimation of JE. Overall, the model by VDW10 together with reasonable assumptions on night-time mixing and the initial evening wind profile provides a good representation of the nocturnal LLJ formation and evolution in form of a parametrization for dust modelling.

## 5. Impact on near-surface winds

### 5.1. Gustiness and the role of shear

The breakdown of the nocturnal LLJ in the morning hours causes an increase in the mean wind speed and a broadening of the wind speed frequency distribution near the surface, which means an



**Figure 7.** Relative frequency distribution of the first-layer wind speed for the LEM run with  $z_0 = 0.01\text{ m}$  at latitude  $20^{\circ}\text{N}$  for different times of day between  $t = 18\text{ h}$  (1800 LT) and  $34\text{ h}$  (1000 LT).

increase in surface gustiness. This is demonstrated in Figure 7 showing line plots of the relative frequency distribution of the one-layer ( $2.6\text{ m}$  above ground) wind speed at different times of day for the model run at  $20^{\circ}\text{N}$  with  $z_0 = 0.01\text{ m}$ . While at

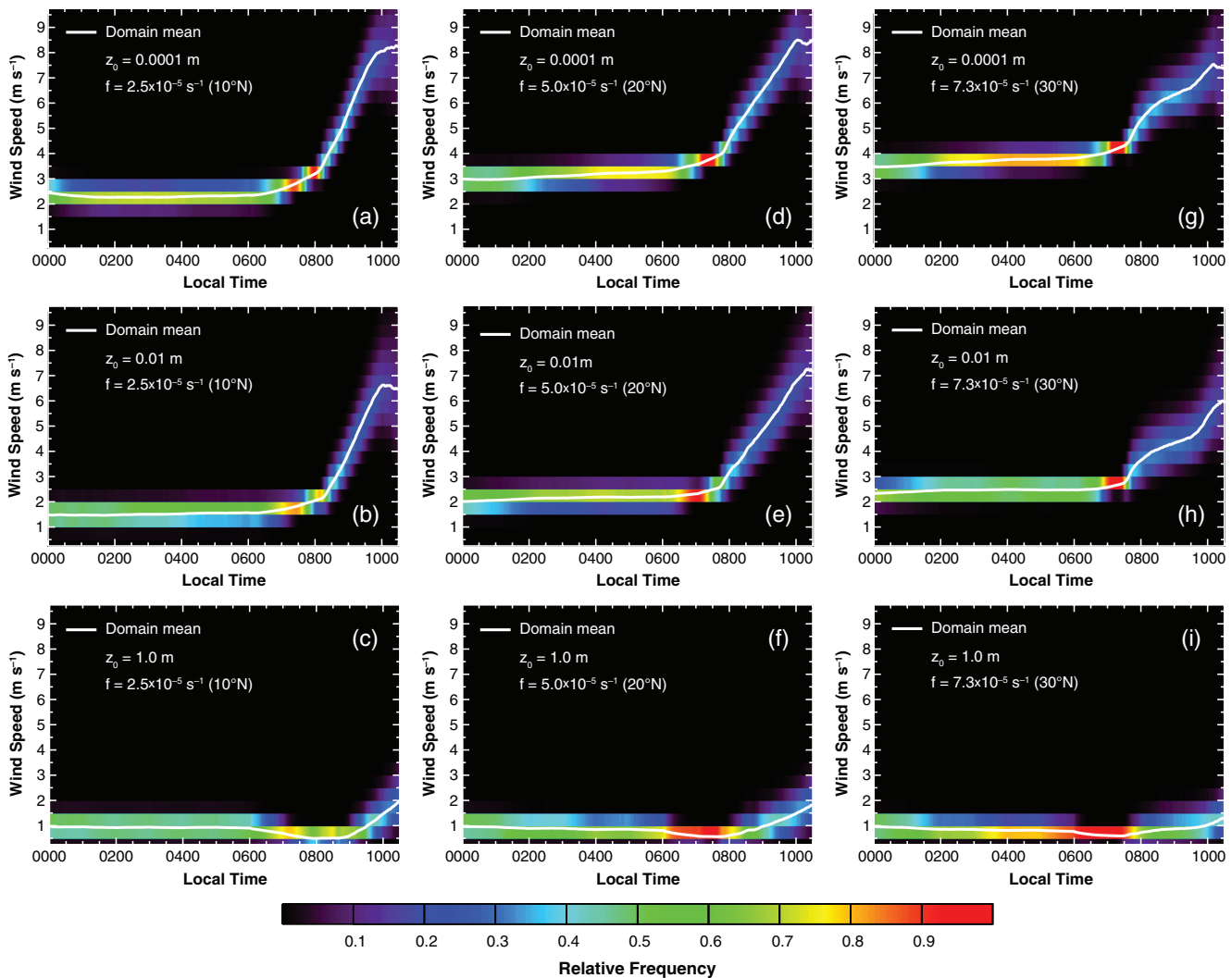


**Figure 8.** Time series of the relative frequency distribution and the domain mean of the first-layer wind speed for different roughness–latitude combinations: (a,d,g)  $z_0 = 0.0001$  m, (b,e,h)  $z_0 = 0.01$  m, (c,f,i)  $z_0 = 1.0$  m, and (a–c)  $10^\circ\text{N}$ , (d–f)  $20^\circ\text{N}$ , (g–i)  $30^\circ\text{N}$  latitude.

night calm conditions prevail with a mean wind speed of about  $2.0 \text{ m s}^{-1}$  and a maximum variability of  $1.0 \text{ m s}^{-1}$  (red and green lines in Figure 7), there is a rapid increase in the mean near-surface winds due to the LLJ breakdown about  $1.5\text{--}2$  h after sunrise. Mean wind speeds increase to values of  $4.7$  and  $6.8 \text{ m s}^{-1}$  at  $0900$  and  $1000$  LT, respectively (blue and yellow lines in Figure 7), as momentum is transferred from the decaying nocturnal LLJ to the ground by turbulent mixing. Because of the stochastic nature of turbulence, this also causes a strong variability in the near-surface wind and a considerable increase in gusts compared to the wind speed distribution of the previous evening (cf. black and orange lines in Figure 7). The morning peaks reach more than  $10 \text{ m s}^{-1}$ , which is well above typical thresholds for mineral dust mobilisation (Marticorena *et al.*, 1995).

Figure 8 shows time series of the modelled relative frequency distribution and the domain mean of the first-layer wind speed for different combinations of surface roughness and geographic latitude. In all cases, the mean near-surface wind speeds are low at night, with values between  $1.0$  and  $3.5 \text{ m s}^{-1}$  and little variability. The night-time wind speeds increase with latitude, for example, from about  $2.5 \text{ m s}^{-1}$  at  $10^\circ\text{N}$  to  $3.5 \text{ m s}^{-1}$  at  $30^\circ\text{N}$  for the model run with  $z_0 = 0.0001$  m (Figure 8(a,d,g)). This is due to the effect of vertical wind shear, which is analysed here using profiles of the gradient Richardson number ( $Ri$ ; Figure 9).

At  $1700$  LT  $Ri$  profiles show typical values for a daytime convective boundary layer (Figure 9(a)). The negative values within the lowest  $50$  m agl indicate that the flow is statically and dynamically unstable, and strong turbulent mixing occurs. One hour after sunset (1900 LT), the thermal stratification has become stable, but dynamically the flow is still unstable, since  $Ri$  is

just larger than zero (Figure 9(b)). Differences between different latitudes are minor.

With increasingly stable conditions, a nocturnal LLJ forms in the course of the night as shown earlier (Figure 4). Two hours after midnight, however, the decoupling from surface friction is still incomplete for  $20^\circ\text{N}$  and in particular for  $30^\circ\text{N}$  latitude despite a similar thermal stratification. Only for the model run at  $10^\circ\text{N}$  is  $Ri$  larger than the critical value ( $Ri_c = 0.25$ ) above which turbulent mixing is suppressed (Figure 9(c)). The reason is that the LLJ oscillation develops much more rapidly at  $30^\circ\text{N}$  compared to  $10^\circ\text{N}$  (Figure 4), which results in significantly stronger wind shear below the jet core. As a consequence, momentum from jet level is permanently mixed down to surface and leads to the higher wind speeds at night (Figure 8).

With increasing surface roughness, near-surface wind speeds at night decrease, and also their increase with latitude is reduced (Figure 8). The effect of surface roughness on stability is shown again by means of  $Ri$  profiles in Figure 9(f–j). As expected, the near-surface flow during the day is more unstable and more turbulent for small roughness lengths (Figure 9(f)), as vertical shear near the surface is large. There is a clear impact of surface roughness on the onset of the evening transition, which occurs considerably later for smaller values of  $z_0$ . While the flow at  $1900$  LT is already statically stable and turbulent mixing tends to cease for  $z_0 = 1.0$  m, convective turbulence remains active for  $z_0 = 0.0001$  m (Figure 9(g)). The resulting delay in frictional decoupling means a shorter period of time for the LLJ to develop until sunrise and, therefore, ultimately causes a weaker jet maximum. Note that for this reason, the LLJ enhancement as defined here is not applicable to very small values of  $z_0$ . As soon

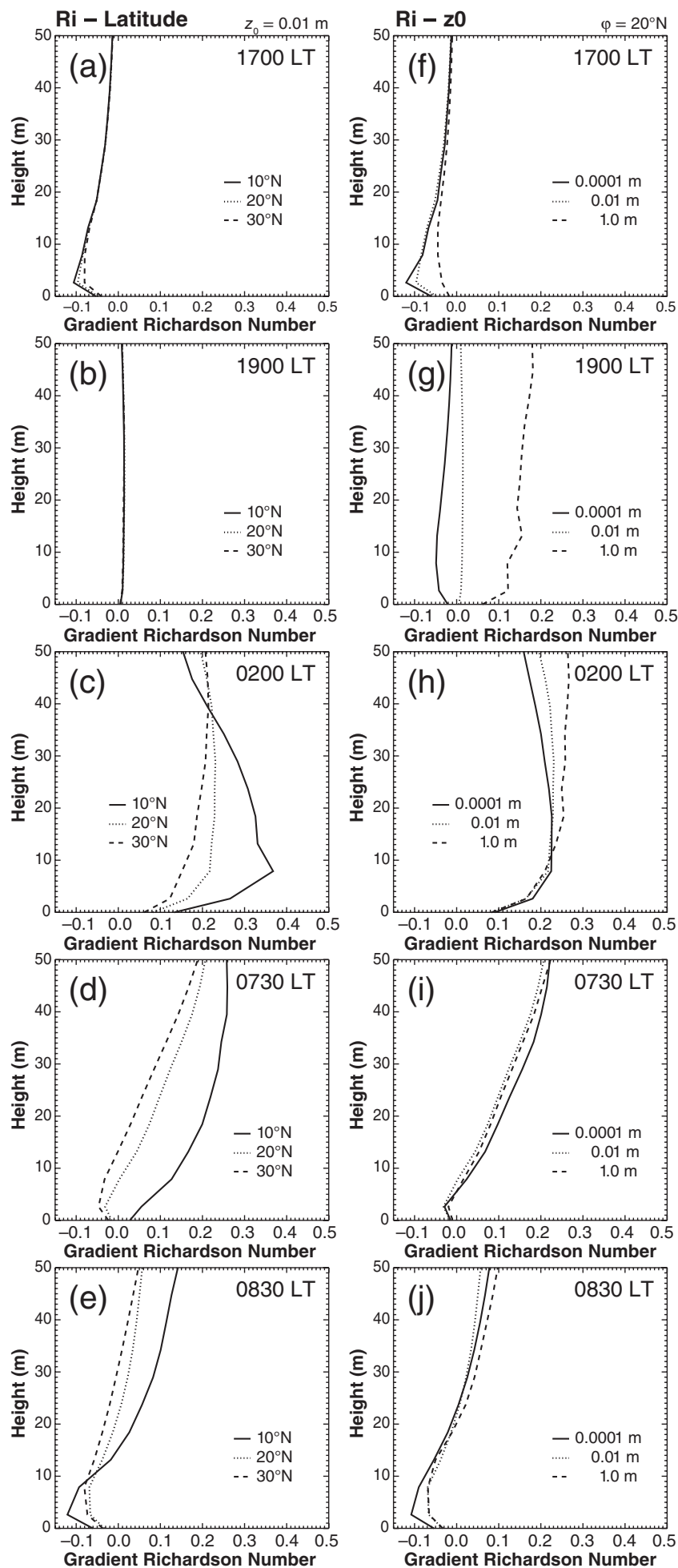


**Figure 9.** Vertical profiles of the gradient Richardson number in dependence of (a–e) latitude (Coriolis parameter) for  $z_0 = 0.01$  m and (f–j) surface roughness at latitude  $20^\circ\text{N}$  for the lowest 50 m from  $t = 17$  h (1700 LT) to 32.5 h (0830 LT).

Table 1. Times of day (LT) for the morning breakdown of LLJs for different roughness–latitude combinations, with 15 min resolution.

Latitude	10°N	20°N	30°N
$z_0$ (m)			
0.0001	0815	0745	0730
0.01	0830	0745	0730
0.1	0845	0800	0730
1.0	0900	0800	0730

as the flow has become decoupled, the effect of surface roughness vanishes, which is reflected in the similarity of  $Ri$  profiles for the different roughness lengths in Figure 9(h,i).

For a short time between 0700 and 0800 LT, the variability in wind speed is further reduced at the onset of the nocturnal LLJ breakdown, which is due to the fact that the turbulent mixing, starting in the surface layer, at first leads to a harmonisation of wind conditions over the model domain. For high values of surface roughness, this causes a decrease in the near-surface wind speed before momentum is mixed down from the nocturnal LLJ and the typical morning peak is formed (Figure 8(c,f,i)). For small roughness lengths, however, this is compensated immediately by momentum transfer from higher layers (Figure 8(a,d,g)). To the best of our knowledge, wind observations (e.g. the diurnal measurements of the near-surface wind speed variability from He *et al.* (2013)) do not show this effect. Therefore, we think that it may be a model artefact due to the transition from the mainly subgrid to the resolved description of near-surface fluxes in the model (see also section 4.1).

The actual time of the morning breakdown varies between 0730 and 0900 LT depending on vertical wind shear and atmospheric stability, which in turn are influenced by latitudinal location and surface roughness, as detailed in Table 1. As described above, the LLJ oscillation is much slower and, thus, wind shear is weaker at 10°N than at 20 or 30°N. Accordingly, the profiles of  $Ri$  for 0730 LT show that atmospheric stratification remains stable for a longer period of time at 10°N latitude. For the higher latitudes, shear-driven turbulence has already lowered the vertical stability during the night, and the morning transition from stable to convective boundary-layer conditions can occur faster (Figure 9(d)). This leads to an evolution where the LLJ breakdown at 10°N occurs later (e.g. 0815 LT for  $z_0 = 0.0001$  m) but is more abrupt and intense, while it is earlier (e.g. 0730 LT for  $z_0 = 0.0001$  m) and more gradual with weaker gusts at 30°N (cf. Figure 8(a,g)). Accordingly, the  $Ri$  profiles for 0830 LT indicate stronger shear instability near the surface for 10°N than for 20 and 30°N latitude (Figure 9(e)).

In addition, the latitude, more precisely the Coriolis parameter, impacts on the phase of the inertial oscillation, which was already discussed in section 4.1. An ideal combination seems to exist for latitudes around 20°N, where almost half of the oscillation period is completed and the jet amplitude is close to maximum in the morning (see also Figure 4(b)), and where shear effects are only moderate. As a result, the highest mean wind speed of about 8.5 m s<sup>-1</sup> and strongest gusts of more than 10.0 m s<sup>-1</sup> are reached for 20°N ( $z_0 = 0.0001$  m) (Figure 8(d)). The considerably slower LLJ evolution and weaker jet maximum at 10°N, however, is largely compensated by a minimum of wind shear, leading to a later and more abrupt LLJ breakdown with stronger gusts (Figure 8(a)).

With increasing roughness length, there is a less significant increase in the mean and the variability of wind speed (Figure 8(a–i)). This is clearly related to the increase in surface friction, dissipating the jet momentum. Furthermore, the breakdown of the nocturnal LLJ tends to occur later with increasing surface roughness (Table 1), since flow conditions are more unstable during the daytime over smoother than over rougher ground. This is reflected by the more negative values of  $Ri$  near surface for  $z_0 = 0.0001$  m compared to the larger roughness

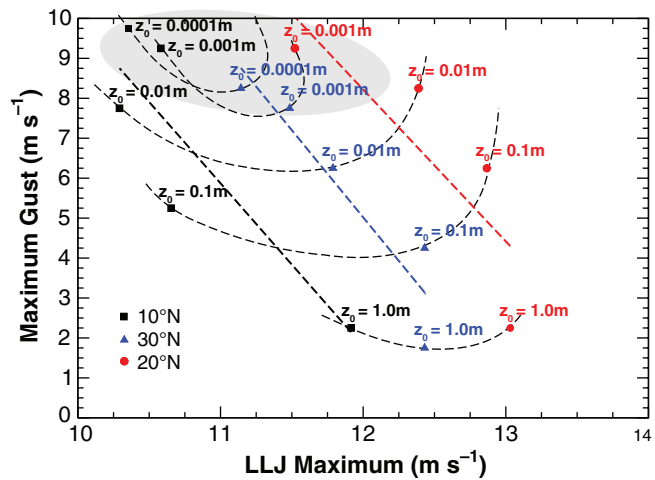


Figure 10. Near-surface gustiness (99% percentile of the 1 min mean one-layer wind speed; see section 5.1) between  $t = 32$  h (0800 LT) and 34 h (1000 LT) in dependence of the LLJ maximum (absolute maximum wind speed at jet level of ca. 100 m agl) for different roughness–latitude combinations. The grey shaded area marks the range of roughness lengths over the Saharan domain shown in Figure 11(a).

lengths in Figure 9(j). The effect is most clear at 10°N latitude, where the time of the LLJ breakdown differs by 45 min between the model runs with  $z_0 = 0.0001$  m (0815 LT) and  $z_0 = 1.0$  m (0900 LT). With increasing latitude, the shift becomes less clear, most likely because shear-driven mixing is already drastically increased at higher latitudes.

The strong mean winds and gusts, in particular, are important drivers of the morning emission of mineral dust. In Figure 10, the dependency of gustiness on the nocturnal LLJ enhancement is analysed in more detail. Shown is the near-surface gustiness between 0800 and 1000 LT against the LLJ's absolute maximum wind speed for specific latitudes and  $z_0$  values. While consistent with JE, here, the LLJ maximum may be the more intuitive measure of jet strength.

In this study, a gust is defined as the 99% percentile of 1 min mean wind speed at the first model level within the 2 h period. While differing from common weather observing practice, this is a well-suited measure of sudden extreme wind events, which has been chosen because of time-resolution limitations of the model output. Although Figure 9 suggests that the LLJ breakdown is not complete at 1000 LT, the analysis is cut off at this time, since later convective eddies tend to grow too large for the model domain, giving unrealistic results.

The maximum gusts obtained this way range from 2.0 to 10.0 m s<sup>-1</sup> for jet maxima of approximately 10.4–13.0 m s<sup>-1</sup>. The strongest LLJs are found around 20°N with a well-balanced, efficient LLJ evolution without important loss of momentum due to shear-induced turbulent mixing, the latter being mainly responsible for weaker jets at 30°N. The weakest LLJs form at 10°N, because of a too-slow development, as discussed in detail in section 4 (Figure 10).

Figure 10 indicates that gustiness tends to decrease with increasing nocturnal LLJ strength. This is surprising at first sight, but mainly results from the effect of surface friction. Hereby, rougher surfaces cause larger ageostrophic wind components and jet amplitudes as well as longer decoupling periods on one hand, but more strongly slow down the near-surface flow on the other hand. With  $z_0 = 1.0$  m the roughness length is still very close to the first-layer height (2.6 m agl), which causes near-surface gusts of only about 2.0 m s<sup>-1</sup> for all latitudes. As surface roughness decreases, the maximum gust increases rapidly. It is remarkable that, for the reasons discussed above, LLJs at 10 and 20°N produce almost similarly strong gusts with 8.3 and 7.8 m s<sup>-1</sup> ( $z_0 = 0.01$  m), respectively, despite different initial jet conditions at the time of breakdown. Significantly weaker gusts are found for each corresponding  $z_0$  for 30°N latitude.

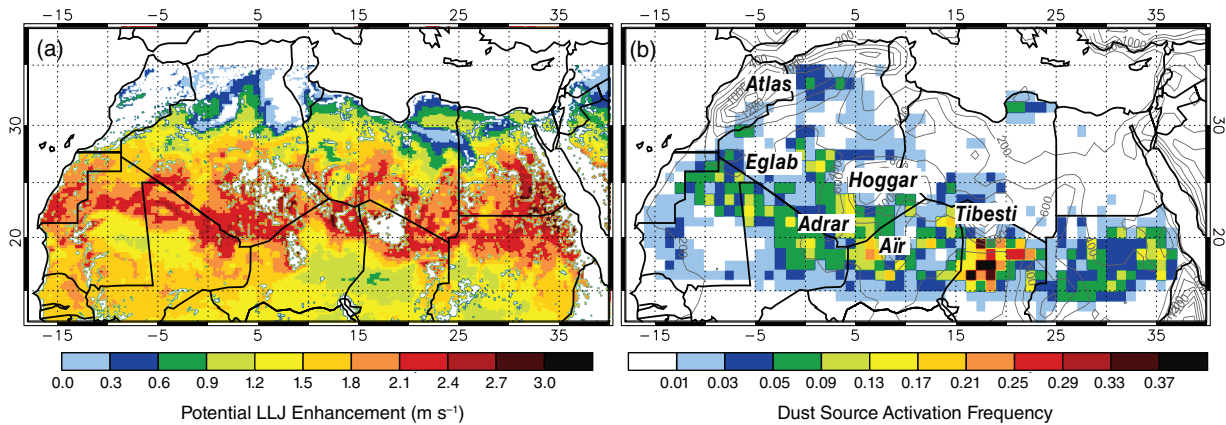


**Figure 11.** (a) Map of potential LLJ enhancement as computed using the statistical relations shown in Figure 5 and satellite retrievals of surface roughness from Prigent *et al.* (2012). Note that a constant geostrophic wind speed [ $U_{\text{geo}}, V_{\text{geo}} = [10.0, 0.0 \text{ m s}^{-1}]$ ] and a fixed diurnal evolution of surface temperature are prescribed for computation. White gaps are due to missing roughness data and grid cells with topographic slopes  $>1\%$ , which are not considered. (b) Map of dust source activation frequency inferred from the 15 min MSG SEVIRI IR dust index for March 2006 to February 2010 (Schepanski *et al.*, 2012).

## 5.2. Geographical distribution and implications for dust emission

Using the relationships for  $JE$  in Eqs (5) and (6), we obtain a map of potential LLJ enhancement for North Africa (Figure 11(a)). The two relationships are combined by translating Eq. (6), so that it equals zero for  $20^\circ\text{N}$ , and then adding it to Eq. (5). For the computation, highly resolved aerodynamic roughness lengths for arid and semi-arid regions at 6 km resolution are used from Prigent *et al.* (2012). The dataset, derived from spaceborne remote sensing, is largely consistent with *in situ*  $z_0$  estimates (90% correlation) and widely used in mineral dust modelling. The satellite-derived roughness data are limited to values smaller than 0.001 m. Higher roughness lengths, which are mainly associated with mountain areas, have significantly lower levels of confidence (for details, see Section 4 in Prigent *et al.* (2012)). The gaps in Figure 11(a) are due to missing roughness data and grid cells in the mountains, where the topographic slope is larger than 1% and, therefore, are not considered to provide optimal conditions for LLJ formation.

Typical values of  $JE$  range from 1.5 to 3.5 m s<sup>-1</sup> assuming a constant geostrophic wind speed of 10 m s<sup>-1</sup> and a spatially fixed diurnal evolution of the surface temperature (for details on the model set-up, see section 2.1). Maximum LLJ enhancements occur in regions between 20 and  $27^\circ\text{N}$  with roughness lengths larger than 0.0001 m, which gives long oscillation periods and strong ageostrophic winds (see section 4.1). The belt of maximum enhancements spans from west Sahara to the Red Sea mountains in the east. North of  $30^\circ\text{N}$ , where  $JE$  is already considerably reduced, individual, less pronounced spots are found south of the Saharan Atlas and over northeast Libya.

High values of surface roughness are mainly related to the foothills of Saharan mountains like the Hoggar and Tibesti Mountains, and the Eglab Massif. These regions have been identified earlier as hot spots of LLJ-related dust events, which is due to the fact that large amounts of loose, fine-grained material are available in the valleys and that orographic channelling and mountain slopes favour the formation of nocturnal LLJs (Holton, 1967; Todd *et al.*, 2008). However, as orographic forcing is not included in this study, Figure 11(a) demonstrates that effects of surface friction and Coriolis forcing play an important role in the LLJ generation in this area. Note that for this reason the potential of the Bodéle LLJ in Chad, a prominent example of a boundary-layer jet in the Sahara (Washington and Todd, 2005), is underestimated here.

In addition to orographic effects, the impact of synoptic-scale forcing (baroclinicity) and heterogeneity in soil moisture and surface heating on the actual occurrence of nocturnal LLJs is not considered and needs further investigation. For example, we would assume that heating curves over the summertime Sahel will deviate significantly from what is shown in Figure 1 due to enhanced soil moisture levels after monsoon rains.

Strong LLJs can cause high peak winds and dust emissions after sunrise, albeit also weak and slowly developing LLJs at low latitudes can produce strong gusts by their more intense breakdowns (see section 5.1, Figure 10). The grey shaded area in Figure 10 marks the range of roughness lengths over the Sahara from the satellite observations. According to this, LLJ strengths of up to 12.0 m s<sup>-1</sup> are sufficient to produce dust-generating gusts larger than typical emission threshold of about 7.0 m s<sup>-1</sup> (Marticorena *et al.*, 1995).

Despite the assumption of constant geostrophic wind and surface forcing, the geographical distribution of  $JE$  in Figure 11(a) agrees surprisingly well with the location of dust source activations as inferred from Meteosat Second Generation Spinning Enhanced Visible and InfraRed Imager (MSG SEVIRI) satellite observations (Figure 11(b)), which are dominated by morning emission events (Schepanski *et al.*, 2007, 2012). The comparison shows that the simple relationships in Eqs (5) and (6) predict strong LLJ breakdowns, where they are in fact observed to occur. These areas also largely coincide with regions that provide soil properties suitable for dust emission. Areas of high dust source activation frequencies, which are covered by the LLJ enhancement, are found in the foothills of the Hoggar and Tibesti Mountains and between the mountain massifs of Eglab, Adrar and Air (see Figure 11(b) for locations). Dust sources located over the Tademaït plateau and the north Sudan, as well as south of the Gulf of Sidra and the Saharan Atlas are also in good agreement with the distribution of  $JE$ . Strong LLJ enhancements in Egypt and the northern Red Sea mountains, however, are not confirmed by the MSG retrieval, while on the other hand, the maximum activation frequencies over the Bodéle Depression are not reflected in  $JE$  for the reason discussed above. Interestingly, the minima of  $JE$  also agree well with minor or no dust source activations as for the gap over central west Mauritania, which is a wide area with low relief.

Encouraged by the good agreement, we would suggest testing the map of potential LLJ enhancement as parametrization for the nocturnal LLJ strength in dust models, which often fail to reproduce morning wind peaks due to the nocturnal LLJ breakdown (e.g. Todd *et al.*, 2008; Fiedler *et al.*, 2013). Since  $JE$  in Figure 11(a) is derived for a constant geostrophic wind speed of 10 m s<sup>-1</sup>, the results would have to be scaled by the model-predicted geostrophic wind or climatological values, and modified according to stability estimates. Such ideas will be explored in future work.

## 6. Summary and discussion

The nocturnal LLJ governs the diurnal cycle of low-level and surface winds, and hence is a key mechanism for dust emission and transport across large parts of the Sahara, the largest source for mineral dust on Earth. For the first time, idealized

large-eddy simulations of the nocturnal LLJ were conducted using the UK Met Office Large-Eddy Model (LEM). Driven by surface temperature observations from a Moroccan field site, the simulations are largely representative for most parts of the Sahara as suggested by satellite data and most likely also for other subtropical deserts. Variations in the synoptic forcing or inhomogeneities in the boundary conditions were not considered.

The model describes the nocturnal LLJ evolution as expected, showing a classical inertial oscillation in the flow above the top of the stable boundary layer. Due to the assumption of barotropicity, the jet maximum is not confined to a shallow layer as often observed, but the flow accelerates across a deep residual layer. The results demonstrate that frictional decoupling during the evening transition and night is well reproduced for the relatively coarse grid spacing (12.5 m). Minor inconsistencies in the jet evolution during the evening transition, however, point towards the need of an even higher spatial resolution, but do not affect the overall conclusions. The morning breakdown of the nocturnal LLJ is also realistic with a considerable increase in near-surface wind speeds.

The idealized settings in this study limit the comparability to observations and to previous LES studies with different model configurations. In accordance with Beare *et al.* (2006a), we show that LESs at 12.5 m spatial resolution are able to sustain resolved turbulence and to produce a well-defined nocturnal SBL. The SBL heights compare well to those in e.g. Beare *et al.* (2006a) and Zhou and Chow (2011), when the differences in the night-time cooling rates are taken into account. Also in agreement with these studies is the strength of modelled nocturnal LLJs, which is on the order of the geostrophic wind speed multiplied by a factor of up to 1.3.

By using a combination of different roughness lengths and latitudinal locations, we investigated the sensitivity of the nocturnal LLJ evolution to surface friction and the Coriolis force. The parameters 'LLJ enhancement' and 'supergeostrophic factor' (difference between the jet-level wind speed at 0600 LT and, respectively, that at 1900 LT and the geostrophic wind speed) were introduced to quantify the potential strength of a nocturnal LLJ in dependence of the two controls investigated. Rougher surfaces cause a stronger drag and higher ageostrophic wind velocities, and therefore larger amplitudes of the nocturnal LLJ oscillation. The Coriolis force controls the phase of the oscillation and, thus, the maximum amplification until the morning breakdown. LLJ enhancements typically range from 1.5 to 3.5 m s<sup>-1</sup>, when a geostrophic wind of 10 m s<sup>-1</sup> and surface homogeneity are assumed. LLJ enhancement and supergeostrophic factor increase approximately logarithmically with surface roughness.

Based on spaceborne estimates of surface roughness, the geographical projection of the potential LLJ enhancement shows that strong nocturnal LLJs can be expected over the Sahara in regions between 20 and 27°N latitude and for roughness lengths larger than 0.0001 m. The patterns agree well with the location of morning dust source activations in MSG SEVIRI satellite observations for the years 2006–2008, supporting the link between the LLJ controls and the observed dust emission.

The simulations confirm the important role of the nocturnal LLJ breakdown as generator of peak near-surface winds during the morning hours. The actual increase in wind speed and variability, however, does not only depend on the LLJ enhancement but also on vertical stability, which is a function of surface friction, wind shear and the Coriolis force. The strongest LLJs producing maximum near-surface gusts are found around 20°N, where a maximum jet amplitude in the morning and only moderate shear effects at night combine in an optimal way. Wind shear lowering the stability overnight is mainly responsible for the poor efficiency of LLJs north of 30°N in generating peak near-surface winds. Remarkably, LLJs at low latitudes compensate a smaller LLJ enhancement by more intense and abrupt breakdowns due to minimum shear-driven mixing, which leads to a more stable nocturnal stratification. Due to larger ageostrophy during daytime, rougher surfaces are associated with

a stronger nocturnal flow enhancement, but generate weaker morning winds at the surface due to a stronger drag. Therefore, the largest LLJ enhancement or absolute strength does not necessarily correspond to the strongest near-surface gusts. Maximum gusts were found for LLJ enhancements of 1.0–2.2 m s<sup>-1</sup> for roughness lengths smaller than 0.01 m.

Similar results regarding the LLJ evolution were found using the theoretical model by VDW10, which describes the nocturnal inertial oscillation starting from a given evening wind profile. The good agreement gives confidence in the LESs but also shows that, for certain purposes, the simple theoretical model provides satisfactory results, if the eddy profile and eddy diffusivity are known during the night, and if shear-induced mixing is not too large. Thus, the VDW10 model could be considered being used as a nocturnal LLJ parametrization in dust modelling.

The assumptions on geostrophic wind and surface temperatures in this idealized modelling study limit the applicability of the results to certain regions and meteorological conditions. The role of orography, surface heterogeneity in soil moisture and surface heating as well as synoptic-scale baroclinicity needs further investigation. Still, the functional relationships derived here for the LLJ enhancement are an important step towards developing a nocturnal LLJ parametrization for large-scale dust models. The results also demonstrate the need of realistically representing the wind speed distribution in dust emission computations.

## Acknowledgements

This work is funded by the European Research Council as part of the 'Desert Storms' project under grant number 257543. We thank Catherine Prigent (CNRS/LERMA, Paris, France) for providing highly resolved aerodynamic roughness data from ASCAT and PARASOL satellite remote sensing, and Eike Bierwirth (University of Leipzig, Germany) for surface temperature measurements at Ouarzazate/Morocco. Kerstin Schepanski (TROPOS, Leipzig, Germany) is thanked for compiling and providing dust source activation frequencies derived from the MSG SEVIRI IR dust index. We acknowledge the usage of ERA-Interim reanalysis data, which is provided by the ECMWF and access granted by the UK Met Office. We would also like to thank Dureid El-Moghraby and Steven Pickering (University of Leeds, UK) for their help in setting up the model as well as two anonymous reviewers for their time and helpful comments on an earlier version of this manuscript.

## References

- Basu S, Holtlag AAM, van de Wiel BJH, Moene AF, Steeneveld GJ. 2008. An inconvenient 'truth' about using sensible heat flux as a surface boundary condition in models under stably stratified regimes. *Acta Geophys.* **56**: 88–99.
- Beare RJ, MacVean MK. 2004. Resolution sensitivity and scaling of large-eddy simulations of the stable boundary layer. *Boundary-Layer Meteorol.* **112**: 257–281.
- Beare RJ, MacVean MK, Holtlag AAM, Cuxart J, Esau I, Golaz JC, Jimenez MA, Khairstdinov M, Kosovic B, Lewellen D, Lund TS, Lundquist JK, McCabe A, Moene AF, Noh Y, Raasch S, Sullivan P. 2006a. An intercomparison of large-eddy simulations of the stable boundary layer. *Boundary-Layer Meteorol.* **118**: 247–272, doi: 10.1007/s10546-004-2820-6.
- Beare RJ, Edwards JM, Lapworth AJ. 2006b. Simulation of the observed evening transition and nocturnal boundary layers: Large-eddy simulation. *Q. J. R. Meteorol. Soc.* **132**: 81–99, doi: 10.1256/qj.05.64.
- Beyrich F, Klose B. 1988. Some aspects of modeling low-level jets. *Boundary-Layer Meteorol.* **43**: 1–14, doi: 10.1007/BF00153966.
- Bierwirth E, Wendisch M, Ehrlich A, Heese B, Tesche M, Althausen D, Schladitz A, Müller D, Otto S, Trautmann T, von Hoyningen-Huene W, Kahn R. 2009. Spectral surface albedo over Morocco and its impact on radiative forcing of Saharan dust. *Tellus B* **61**: 252–269, doi: 10.1111/j.1600-0889.2008.00395.x.
- Blackadar AK. 1957. Boundary layer wind maxima and their significance for the growth of nocturnal inversions. *Bull. Am. Meteorol. Soc.* **38**: 283–290.
- Bonner WD. 1968. Climatology of the low level jet. *Mon. Weather Rev.* **96**: 833–850.
- Bonner WD, Paegle J. 1970. Diurnal variations in boundary layer winds over the south-central United States in summer. *Mon. Weather Rev.* **98**: 735–744, doi: 10.1175/1520-0493(1970)098<0735:DVLW>2.3.CO;2.

- Bosveld FC, Baas P, Steeneveld GJ, Holtslag AAM, Angevine WM, Bazile E, de Brujin EIF, Deacu D, Edwards JM, Ek M, Larson VE, Pleim JE, Raschendorfer M, Svensson G. 2014. The GABLS third intercomparison case for model evaluation. Part B: SCM model intercomparison and evaluation. *Boundary-Layer Meteorol.* **152**: 157–187, doi: 10.1007/s10546-014-9919-1.
- Cheinet S, Beljaars A, Köhler M, Morcrette JJ, Viterbo P. 2005. *Validating Physical Processes in the ECMWF Forecasts Through the ARM SGP Site Measurements, ECMWF-ARM Technical Memorandum 1*. ECMWF: Reading, UK.
- Cuesta J, Marsham JH, Parker DJ, Flamant C. 2009. Dynamical mechanisms controlling the vertical redistribution of dust and the thermodynamic structure of the west Saharan atmospheric boundary layer during summer. *Atmos. Sci. Lett.* **10**: 34–42, doi: 10.1002/asl.207.
- Cuxart J, Jiménez MA. 2007. Mixing processes in a nocturnal low-level jet: An LES study. *J. Atmos. Sci.* **64**: 1666–1679, doi: 10.1175/JAS3903.1.
- Darby LS, Allwine KJ, Banta RM. 2006. Nocturnal low-level jet in a mountain basin complex. Part II: Transport and diffusion of tracer under stable conditions. *J. Appl. Meteorol. Clim.* **45**: 740–753, doi: 10.1175/JAM2367.1.
- Fiedler S, Schepanski K, Heinold B, Knippertz P, Tegen I. 2013. Climatology of nocturnal low-level jets over North Africa and implications for modeling mineral dust emission. *J. Geophys. Res. Atmos.* **118**: 6100–6121, doi: 10.1002/jgrd.50394.
- Gamo M. 1996. Thickness of the dry convection and large-scale subsidence above deserts. *Boundary-Layer Meteorol.* **79**: 265–278, doi: 10.1007/BF00119441.
- Gray MEB, Petch J, Derbyshire SH, Brown AR, Lock AP, Swann HA, Brown PRA. 2001. Version 2.3 of the Met Office large eddy model. Part II: Scientific documentation, Technical Report 49. Met Office: Bracknell, UK. <http://appconv.metoffice.com/LEM/docs/Scientific.ps> (accessed 13 January 2011).
- He YP, Monahan AH, McFarlane NA. 2013. Diurnal variations of land surface wind speed probability distributions under clear-sky and low-cloud conditions. *Geophys. Res. Lett.* **40**: 3308–3314, doi: 10.1002/grl.50575.
- Heinold B, Knippertz P, Marsham JH, Fiedler S, Dixon NS, Schepanski K, Laurent B, Tegen I. 2013. The role of deep convection and nocturnal low-level jets for dust emission in summertime West Africa: Estimates from convection-permitting simulations. *J. Geophys. Res. Atmos.* **118**: 4385–4400, doi: 10.1002/jgrd.50402.
- Holton JR. 1967. The diurnal boundary layer wind oscillation above sloping terrain. *Tellus* **19**: 199–205.
- Holtslag AAM. 2006. GEWEX Atmospheric Boundary-Layer Study (GABLS) on stable boundary layers. *Boundary-Layer Meteorol.* **118**: 243–246, doi: 10.1007/s10546-005-9008-6.
- Jin M, Dickinson RE. 2010. Land surface skin temperature climatology: Benefiting from the strengths of satellite observations. *Environ. Res. Lett.* **5**: 4004, doi: 10.1088/1748-9326/5/4/044004.
- Knippertz P. 2008. Dust emissions in the West African heat trough – the role of the diurnal cycle and of extratropical disturbances. *Meteorol. Z.* **17**: 553–563, doi: 10.1127/0941-2948/2008/0315.
- Knippertz P, Todd MC. 2012. Mineral dust aerosol over the Sahara: Meteorological controls on emission and transport and implications for modelling. *Rev. Geophys.* **50**: RG1007, doi: 10.1029/2011RG000362.
- Koren I, Kaufman YJ, Washington R, Todd MC, Rudich Y, Martins VJ, Rosenfeld D. 2006. The Bodélé depression – a single spot in the Sahara that provides most of the mineral dust to the Amazon forest. *Environ. Res. Lett.* **1**: 014005, doi: 10.1088/1748-9326/1/1/014005.
- Kosović B, Curry JA. 2000. A large eddy simulation study of a quasi-steady, stably stratified atmospheric boundary layer. *J. Atmos. Sci.* **57**: 1052–1068, doi: 10.1175/1520-0469(2000)057<1052:ALESSO>2.0.CO;2.
- Lilly DK. 1967. The representation of small-scale turbulence in numerical simulation experiments. In *Proceedings, IBM Scientific Computing Symposium on Environmental Sciences*, 1966, November 14–16, Goldstein HH (ed.): 195–210. Thomas J. Watson Research Center: Yorktown Heights, New York, NY.
- Mahrt L. 2008. The influence of transient flow distortion on turbulence in stable weak-wind conditions. *Boundary-Layer Meteorol.* **127**: 1–16, doi: 10.1007/s10546-007-9244-z.
- McNider RT, Moran MD, Pielke RA. 1988. Influence of diurnal and inertial boundary-layer oscillations on long range dispersion. *Atmos. Environ.* **22**: 2445–2462, doi: 10.1016/0004-6981(88)90476-3.
- Mao H, Talbot R. 2004. Role of meteorological processes in two New England ozone episodes during summer 2001. *J. Geophys. Res.* **109**: D20305, doi: 10.1029/2004JD004850.
- Marsham JH, Hobby M, Allen CJT, Banks JR, Bart M, Brooks BJ, Cavazos-Guerra C, Hobby M, Allen CJT, Banks JR, Bart M, Brooks BJ, Cavazos-Guerra C, Engelstaedter GS, Gascoyne M, Lima AR, Martins JV, McQuaid JB, O'Leary A, Ouchene B, Ouladichir A, Parker DJ, Saci A, Salah-Ferroudji M, Todd MC, Washington R. 2013. Meteorology and dust in the central Sahara: Observations from Fennec supersite-1 during the June 2011 intensive observation period. *J. Geophys. Res. Atmos.* **118**: 4069–4089, doi: 10.1002/jgrd.50211.
- Marticorena B, Bergametti G. 1995. Modeling the atmospheric dust cycle: 1. Design of a soil-derived dust emission scheme. *J. Geophys. Res. Atmos.* **100**: 16415–16430, doi: 10.1029/95JD00690.
- May PT. 1995. The Australian nocturnal jet and diurnal variations of boundary-layer winds over Mt. Isa in north-eastern Australia. *Q. J. R. Meteorol. Soc.* **121**: 987–1003, doi: 10.1002/qj.49712152503.
- Newsom RK, Banta RM. 2003. Shear-flow instability in the stable nocturnal boundary layer as observed by Doppler lidar during CASES-99. *J. Atmos. Sci.* **60**: 16–33, doi: 10.1175/1520-0469(2003)060<0016:SFIITS>2.0.CO;2.
- Piacsek SA, Williams GP. 1970. Conservation properties of convection difference schemes. *J. Comput. Phys.* **198**: 580–616.
- Pinker RT, Sun D, Miller M, Robinson GJ. 2007. Diurnal cycle of land surface temperature in a desert encroachment zone as observed from satellites. *Geophys. Res. Lett.* **34**: L11809, doi: 10.1029/2007GL030186.
- Prigent C, Jiménez C, Catherinot J. 2012. Comparison of satellite microwave backscattering (ASCAT) and visible/near-infrared reflectances (PARASOL) for the estimation of aeolian aerodynamic roughness length in arid and semi-arid regions. *Atmos. Meas. Tech.* **5**: 2703–2712, doi: 10.5194/amt-5-2703-2012.
- Rife DL, Pinto JO, Monaghan AJ, Davis CA, Hannan JR. 2010. Global distribution and characteristics of diurnally varying lowlevel jets. *J. Clim.* **23**: 5041–5064, doi: 10.1175/2010JCLI3514.1.
- Sandu I, Beljaars A, Bechtold P, Mauritzen T, Balsamo G. 2013. Why is it so difficult to represent stably stratified conditions in numerical weather prediction (NWP) models? *J. Adv. Model. Earth Syst.* **5**: 117–133, doi: 10.1002/jame.20013.
- Schepanski K, Tegen I, Laurent B, Heinold B, Macke A. 2007. A new Saharan dust source activation frequency map derived from MSG-SEVIRI IR-channels. *Geophys. Res. Lett.* **34**: L18803, doi: 10.1029/2007GL030168.
- Schepanski K, Tegen I, Todd MC, Heinold B, Boenisch G, Laurent B, Macke A. 2009. Meteorological processes forcing Saharan dust emission inferred from MSG-SEVIRI observations of subdaily dust source activation and numerical models. *J. Geophys. Res. Atmos.* **114**: D10201, doi: 10.1029/2008JD010325.
- Schepanski K, Tegen I, Macke A. 2012. Comparison of satellite based observations of Saharan dust source areas. *Remote Sens. Environ.* **123**: 90–97, doi: 10.1016/j.rse.2012.03.019.
- Shapiro A, Fedorovich E. 2009. Nocturnal low-level jet over a shallow slope. *Acta Geophys.* **57**: 950–980, doi: 10.2478/s11600-009-0026-5.
- Shapiro A, Fedorovich E. 2010. Analytical description of a nocturnal low-level jet. *Q. J. R. Meteorol. Soc.* **136**: 1255–1262, doi: 10.1002/qj.628.
- Singh MP, McNider RT, Lin JT. 1993. An analytical study of diurnal wind-structure variations in the boundary layer and the low-level nocturnal jet. *Boundary-Layer Meteorol.* **63**: 397–423, doi: 10.1007/BF00705360.
- Stensrud DJ. 1996. Importance of low-level jets to climate: A review. *J. Clim.* **9**: 1698–1711, doi: 10.1175/1520-0442(1996)009<1698:IOLLJT>2.0.CO;2.
- Storm B, Dudhia J, Basu S, Swift A, Giammanco I. 2009. Evaluation of the Weather Research and Forecasting model on forecasting low-level jets: Implication for wind energy. *Wind Energy* **12**: 81–90, doi: 10.1002/we.288.
- Sun JL, Lenschow DH, Burns SP, Banta RM, Newsom RK, Coulter R, Frasier S, Ince T, Nappo C, Balsley BB, Jensen M, Mahrt L, Miller D, Skelly B. 2004. Atmospheric disturbances that generate intermittent turbulence in nocturnal boundary layers. *Boundary-Layer Meteorol.* **110**: 255–279, doi: 10.1023/A:1026097926169.
- Thorpe AJ, Guymer TH. 1977. The nocturnal jet. *Q. J. R. Meteorol. Soc.* **103**: 633–653, doi: 10.1002/qj.49710343809.
- Todd MC, Bou Karam D, Cavazos C, Bouet C, Heinold B, Baldasano JM, Cautenet G, Koren I, Perez C, Solmon F, Tegen I, Tulet P, Washington R, Zakey A. 2008. Quantifying uncertainty in estimates of mineral dust flux: An intercomparison of model performance over the Bodélé Depression, northern Chad. *J. Geophys. Res.* **113**: D24107, doi: 10.1029/2008JD010476.
- Van de Wiel BJH, Moene AF, Steeneveld GJ, Baas P, Bosveld FC, Holtslag AAM. 2010. A conceptual view on inertial oscillations and nocturnal low-level jets. *J. Atmos. Sci.* **67**: 2679–2689, doi: 10.1175/2010JAS3289.1.
- Washington R, Todd MC. 2005. Atmospheric controls on mineral dust emission from the Bodélé Depression, Chad: The role of the low level jet. *Geophys. Res. Lett.* **32**: L17701, doi: 10.1029/2005GL023597.
- Wittich KP, Hartmann J, Roth R. 1986. On nocturnal wind shear with a view to engineering applications. *Boundary-Layer Meteorol.* **37**: 215–227, doi: 10.1007/BF00122985.
- Zhang DL, Zheng WZ. 2004. Diurnal cycles of surface winds and temperatures as simulated by five boundary layer parameterisations. *J. Appl. Meteorol.* **43**: 157–169, doi: 10.1175/1520-0450(2004)043<0157:DCOSWA>2.0.CO;2.
- Zhou BW, Chow FK. 2011. Large-eddy simulation of the stable boundary layer with explicit filtering and reconstruction turbulence modeling. *J. Atmos. Sci.* **68**: 2142–2155, doi: 10.1175/2011JAS3693.1.